DOI: 10.1002/ejic.200600705

Reactions of GaCp* with a Hemilabile Derivative of $Rh_6(CO)_{16}$ – Synthesis and Structural Characterization of Two Novel Heterometallic Clusters: $Rh_6(CO)_{13}$-(μ,κ^3-$Ph_2PC_2H_3$)(μ_3-GaCp*) and $Rh_6(CO)_{13}$(κ^1-$Ph_2PC_2H_3$)(μ_3-GaCp*)$_2$

Elena V. Grachova,[a] Gerald Linti,[b] Hans-Georg Stammler,[c] Beate Neumann,[c] Sergey P. Tunik,*[a] and Hubert Wadepohl[b]

Keywords: Cluster compounds / Heterometallic complexes / Phosphane ligands

The reaction of $Rh_6(CO)_{14}(Ph_2PCH{=}CH_2)$ with a twofold excess of GaCp* (Cp* = C_5Me_5) affords two novel heterometallic clusters $Rh_6(CO)_{13}(\mu,\kappa^3\text{-}Ph_2PC_2H_3)(\mu_3\text{-}GaCp^*)$ (**1**) and $Rh_6(CO)_{13}(\kappa^1\text{-}Ph_2PC_2H_3)(\mu_3\text{-}GaCp^*)_2$ (**2**) in a moderate yield. The hemilabile behavior of coordinated diphenylvinylphosphane in the starting cluster allows the easy insertion of GaCp* into the cluster coordination sphere, which eventually gives the cluster **1** with face-bridging coordination of the gallium fragment and the phosphane ligand recoordinated in an edge-bridging position. The further substitution of the vinyl function in **1** for the second GaCp* ligand affords cluster **2**, where recoordination of the double bond is blocked by steric hindrance from adjacent GaCp* fragments. Both clusters were structurally characterized by X-ray crystallography in the solid state and by IR and NMR spectroscopy in solution. Hemilability of diphenylvinylphosphane in **1** was independently confirmed by the cluster reaction with CO, which gives the $Rh_6(CO)_{14}(\kappa^1\text{-}Ph_2PC_2H_3)(GaCp^*)$ adduct (**3**) with the phosphane ligand only coordinated through the phosphorus atom.

Introduction

Syntheses of heterometallic complexes with a direct bond between transition and nontransition metals has attracted considerable attention because of their unusual physico–chemical properties and their potential application in material science.[1–3] In this area the chemistry of gallium containing compounds has been significantly developed over the last years owing to the use of GaCp* as a ligand in the coordination chemistry of mono-[4–8] and polynuclear[9–12] complexes. Recently we reported the synthesis and structural characterization[13,14] of a series of "very-mixed-metal" clusters containing GaCp* fragments in μ_3- and μ_2-bridging positions over the Rh_6 and $Ru_6(C)$ metal frameworks. An extension of these studies in our laboratory was aimed at the modification of the cluster properties through further substitution of CO for such typically modifying ligands as the phosphanes. However, neither of the straightforward approaches, reactions of the phosphane substituted derivatives with GaCp* or treatment of the gallium containing clusters with phosphanes, gave positive results. To explore this chemistry further we attempted to prepare analogous heterometallic complexes using a hemilabile phosphanyl-alkenyl derivative of the $Rh_6(CO)_{16}$ cluster.[15] In general, the hemilabile ligands in cluster compounds facilitate substitution reactions and make it possible to direct the coordination of an incoming ligand to the position initially occupied by the labile function that determines the stereochemistry of the substituted product and mode of transformation of the coordinated substrate.[16–18] This approach proved to be successful and in this paper we report on the synthesis, structural characterization, and reactivity of three novel clusters: $Rh_6(CO)_{13}(\mu,\kappa^3\text{-}Ph_2PC_2H_3)(\mu_3\text{-}GaCp^*)$ (**1**), $Rh_6(CO)_{13}(\kappa^1\text{-}Ph_2PC_2H_3)(\mu_3\text{-}GaCp^*)_2$ (**2**), and $Rh_6(CO)_{14}(\kappa^1\text{-}Ph_2PC_2H_3)(GaCp^*)$ (**3**).

Results and Discussion

The low temperature reaction of the starting $Rh_6(CO)_{14}(\mu,\kappa^3\text{-}Ph_2PC_2H_3)$ cluster with a twofold excess of GaCp* gives a mixture of the $Rh_6(CO)_{13}(\mu,\kappa^3\text{-}Ph_2PC_2H_3)(\mu_3\text{-}GaCp^*)$ (**1**) and $Rh_6(CO)_{13}(\kappa^1\text{-}Ph_2PC_2H_3)(\mu_3\text{-}GaCp^*)_2$ (**2**) clusters together with $Rh_6(CO)_{16-x}(GaCp^*)_x$ derivatives, and the latter were identified by their characteristic IR spectra.[13,14] Solid-state structures of **1** and **2** were established by X-ray crystallographic analysis. Selected structural pa-

[a] Department of Chemistry, St. Petersburg State University, Universitetskii pr. 26, 198504 St. Petersburg, Russia
Fax: +7-812-428-6939
E-mail: stunik@chem.spbu.ru
[b] Anorganisch-Chemisches Institut, Ruprecht-Karls-Universität Heidelberg,
Im Neuenheimer Feld 270, 69120 Heidelberg, Germany
[c] Fakultät für Chemie, Universität Bielefeld,
Universitätsstraße 25, 33615 Bielefeld, Germany
Supporting information for this article is available on the WWW under http://www.eurjic.org or from the author.

rameters of these molecules are given in Table 1, ORTEP views of **1** and **2** are shown in Figures 1 and 3, respectively.

The crystal structure of the cluster **1** appears disordered because of the presence of two isomers (approximate ratio 7:3), which differ in the orientation of the "$PhPCH{=}CH_2$" moiety with respect to the Rh_3 triangle it is coordinated to. The remaining part of the molecule is essentially identical for both isomers. The molecule of **1** consists of a Rh_6 octahedron with a face-bridging GaCp* and an edge-bridging μ,κ^3-diphenylvinylphosphane coordinated over opposite faces of the octahedron. The ligand shell of the metal cluster is completed by three face-bridging and ten terminal CO

Table 1. Selected bond lengths [Å] and angles [°] for **1** and **2**.

	$Rh_6(CO)_{13}(Ph_2PC_2H_3)(GaCp^*)$, 1				**$Rh_6(CO)_{13}(Ph_2PC_2H_3)(GaCp^*)_2$, 2**	
Rh Rh triangles capped by GaCp*	Rh(1) Rh(2)	2.8746(4)			Rh(1) Rh(2)	2.8317(3)
	Rh(1) Rh(3)	2.8123(4)			Rh(1) Rh(3)	2.7920(3)
	Rh(2) Rh(3)	2.8021(4)			Rh(1) Rh(4)	2.8431(3)
					Rh(1) Rh(5)	2.8508(3)
					Rh(2) Rh(3)	2.8418(3)
					Rh(4) Rh(5)	2.7859(3)
Average[a]		**2.8297(0.0320)**				**2.8242(0.0256)**
Rh Rh bonds remote to GaCp*	Rh(1) Rh(4)	2.7380(3)	Rh(1) Rh(6)	2.7428(3)	Rh(2) Rh(5)	2.7526(3)
	Rh(2) Rh(4)	2.7495(3)	Rh(2) Rh(5)	2.7587(3)	Rh(2) Rh(6)	2.7556(3)
	Rh(3) Rh(5)	2.7810(3)	Rh(3) Rh(6)	2.8016(3)	Rh(3) Rh(4)	2.7815(3)
	Rh(4) Rh(5)	2.7814(4)	Rh(4) Rh(6)	2.7821(4)	Rh(3) Rh(6)	2.7698(3)
	Rh(5) Rh(6)	2.7065(3)			Rh(4) Rh(6)	2.7933(3)
					Rh(5) Rh(6)	2.8459(3)
Average[a]				**2.7602(0.0276)**		**2.7831(0.0314)**
Rh–(μ_3-CO) bond length	C(21) Rh(2)	2.305(3)	C(22) Rh(1)	2.192(3)	C(25) Rh(2)	2.244(3)
	C(21) Rh(4)	2.203(3)	C(22) Rh(4)	2.204(3)	C(25) Rh(5)	2.161(3)
	C(21) Rh(5)	2.102(3)	C(22) Rh(6)	2.130(3)	C(25) Rh(6)	2.117(3)
	C(23) Rh(3)	2.100(3)			C(28) Rh(3)	2.206(3)
	C(23) Rh(5)	2.153(3)			C(28) Rh(4)	2.182(3)
	C(23) Rh(6)	2.282(3)			C(28) Rh(6)	2.155(3)
	Major isomer		**Minor isomer**			
Bond lengths and angles in the $Ph_2PC_2H_3$ ligand	Rh(5) P(1a)	2.260(5)	Rh(5) P(1b)	2.351(11)	Rh(6) P(1)	2.3416(8)
	Rh(6) C(25a)	2.267(4)	Rh(6) C(25b)	2.193(9)	P(1) C(34)	1.809(3)
	Rh(6) C(24a)	2.231(4)	Rh(6) C(24b)	2.225(9)	C(34) C(35)	1.314(5)
	P(1a) C(25a)	1.812(6)	P(1b) C(25b)	1.807(16)	Rh(6) P(1) C(34)	115.51(10)
	C(24a) C(25a)	1.384(7)	C(24b) C(25b)	1.338(16)	P(1) C(34) C(35)	124.8(3)
	Rh(5) P(1a) C(25a)	101.6(2)	Rh(5) P(1b) C(25b)	103.4(6)		
	P(1a) C(25a) C(24a)	125.7(4)	P(1b) C(25b) C(24b)	125.3(11)		
Non-bonding contacts of the $Ph_2PC_2H_3$ ligand and μ_3-CO	C(22) H(24a)	2.656	C(22) H(26b)	2.885		
	C(23) C(25a)	2.834	C(23) H(24b)	2.750		
	C(23) H(26a)	2.717	O(23) H(24b)	2.635		
	O(23) H(26a)	2.646				
	$Rh_6(CO)_{13}(Ph_2PC_2H_3)(GaCp^*)$, 1		**$Rh_6(CO)_{13}(Ph_2PC_2H_3)(GaCp^*)_2$, 2**			
Ga–Rh bond lengths	Ga(1) Rh(1)	2.5800(4)	Ga(1) Rh(1)	2.5835(4)	Ga(2) Rh(1)	2.5214(4)
	Ga(1) Rh(2)	2.5508(4)	Ga(1) Rh(2)	2.5441(4)	Ga(2) Rh(4)	2.5886(4)
	Ga(1) Rh(3)	2.5789(4)	Ga(1) Rh(3)	2.5703(4)	Ga(2) Rh(5)	2.5822(4)
Ga $C_{centroid}$	Ga(1) $C_{centroid}$	1.978	Ga(1) $C_{centroid}$	1.994	Ga(2) $C_{centroid}$	2.041
Ga $Rh_{triangle}$	Ga(1) $Rh_{triangle}$	1.984	Ga(1) $Rh_{triangle}$	1.982	Ga(2) $Rh_{triangle}$	1.978
$C_{centroid}$ Ga $Rh_{triangle}$	$C_{centroid}$ Ga(1) $Rh_{triangle}$	177.98	$C_{centroid}$ Ga(1) $Rh_{triangle}$	177.35		
			$C_{centroid}$ Ga(2) $Rh_{triangle}$	171.75		

[a] Values of standard deviations are given in brackets.

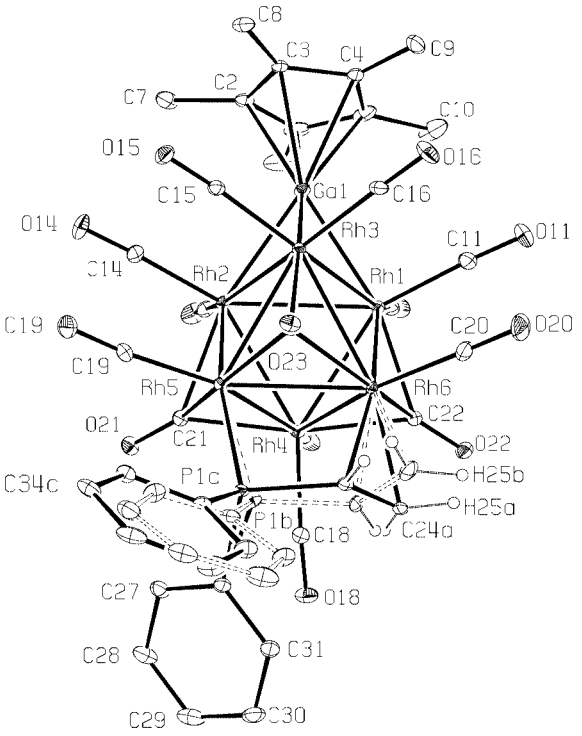

Figure 1. The ORTEP view of the $Rh_6(CO)_{13}(\mu,\kappa^3\text{-}Ph_2PC_2H_3)(\mu_3\text{-}GaCp^*)$ (**1**). Thermal ellipsoids are drawn at the 50% level.

ligands. The stoichiometry of **1** results in 86 valence electrons, which is consistent with the *closo* octahedral structure of the metal framework[19,20] as in the parent $Rh_6(CO)_{16}$[21] and its substituted derivatives.[15,21–24] The general structural motif of **1** is closely analogous to that of $[Rh_6(CO)_{14}(\mu,\kappa^3\text{-}Ph_2PC_2H_3)]$[15] apart from the presence of the GaCp* fragment in **1** instead of a face-bridging CO.

The effects of both substituting ligands ($Ph_2PC_2H_3$ and GaCp*) are nearly independent and their influence is observed in the vicinity of the substitution sites, see Table 1. Coordination of the short-bite vinylphosphane moiety results in contraction of the Rh–Rh edge spanned by the phosphane ligand. This bond is the shortest [2.7065(3) Å] metal–metal distance in the molecule. Very similar to the monosubstituted $Rh_6(CO)_{15}GaCp^*$ cluster[13] the metal–metal bonds in the rhodium triangle capped by the gallium ligand are considerably elongated. This is a typical electronic effect of the weak π acceptor and was found earlier in the clusters $Rh_6(CO)_{16-x}(GaCp^*)_x$[13] and $Ru_6(C)(CO)_{17-x}(GaCp^*)_x$.[14] The Ga–Rh distances fall into quite a narrow range (2.551–2.580 Å), which indicates an essentially symmetric coordination of the GaCp* moiety to the rhodium triangle.

The two isomers of **1** differ in the orientation of the P–C=C fragment of the vinylphosphane ligand relative to the Rh(4)Rh(5)Rh(6) triangle, Figure 2. In the major isomer the Rh–P distance [2.260(5) Å] is considerably shorter [cf. 2.351(11) Å in the minor species], which is indicative of a stronger metal-to-phosphorus bonding. A comparison of the angular parameters that characterize the P–Rh(5) interaction also points to a less strained bonding mode of the phosphorus atom to the octahedral framework in the major isomer. The Rh(4)–Rh(5)–P and Rh(6)–Rh(5)–P angles are equal to 96.8° and 78.0° (major isomer), and 88.3° and 73.8° (minor isomer), whereas the *cis* Rh–Rh–C(O) angles in the parent (unstrained) $Rh_6(CO)_{16}$ are equal to ca. 97°.[21] On the contrary, distances from the carbon atoms of the coordinated vinyl moiety to Rh(6) are somewhat longer in the major species (Table 1), which is evidently a geometrical consequence of the strong phosphorus-to-rhodium bond mentioned above. Similar to the $Rh_6(CO)_{14}(\mu,\kappa^3\text{-}Ph_2PC_2H_3)$ cluster[15] both isomers display short (<2.9 Å) nonbonding contacts between atoms of the vinyl fragment and adjacent face-bridging C(22)O and C(23)O ligands. This steric hindrance results in the shift of the C(23)O group from the substituted Rh(5) and Rh(6) centers to Rh(3), opposite to the regular shift caused by the electronic effect of a heteroligand.[15,21,22,25] It is worth noting that the present crystallographic study, which revealed two conformations of the P–C=C fragment in the solid-state structure of **1**, independently confirmed the structural models of the $Rh_6(CO)_{14}(\mu,\kappa^3\text{-}Ph_2PC_2H_3)$ isomers suggested in our earlier work, which was solely based on NMR spectroscopic data.[15] The disposition of the vinyl moiety over the metal triangle in the minor conformer of the parent $Rh_6(CO)_{14}(\mu,\kappa^3\text{-}Ph_2PC_2H_3)$ cluster[15] matches well the structural pattern shown in part b of Figure 2.

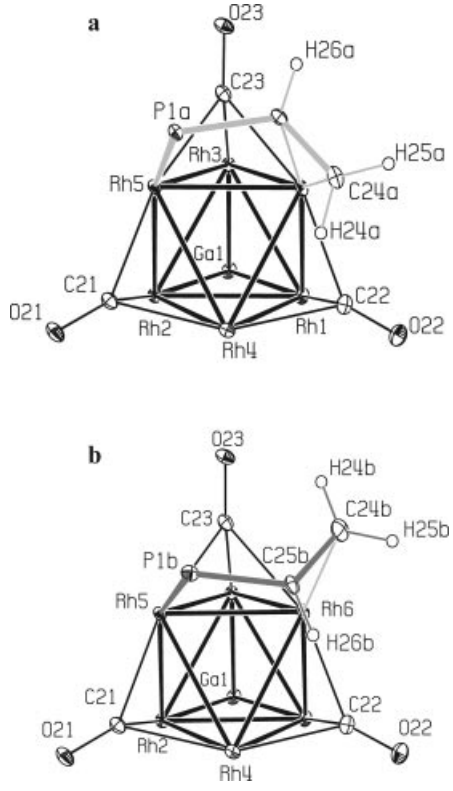

Figure 2. Two isomers of the **1** cluster; (a) major isomer, (b) minor isomer. For the sake of simplicity terminal CO ligands are omitted.

The ^1H and ^{31}P NMR spectroscopic study of **1** showed that in solution this cluster exists as a mixture of two isomers, the structures of which obviously match those found

in the solid state. The chemical shifts and coupling constants of the signals observed in the ^1H spectrum are completely consistent with the data obtained earlier for the conformers of $Rh_6(CO)_{14}(\mu,\kappa^3\text{-}Ph_2PC_2H_3)$.[15] It is also worth noting that the Rh–P coupling constants of the isomers of **1** are in agreement with the Rh–P bond lengths in these species. The stronger Rh–P bond in the major isomer gives rise to a higher value of the corresponding coupling constant. These two forms of the vinyl fragment coordination easily convert into each other; the rate of the dynamic process is slow at 273 K and gives the low-temperature-limiting spectrum shown in Figure S1 (S denotes data in Supporting Information file). The resonances from the minor isomer broaden on heating and eventually disappear into the baseline at 313 K. This behavior is very similar to the dynamics observed in $Rh_6(CO)_{14}(\mu,\kappa^3\text{-}Ph_2PC_2H_3)$,[15] however, the exchange rate in the latter case is slightly higher.

The $Rh_6(CO)_{13}(\kappa^1\text{-}Ph_2PC_2H_3)(\mu_3\text{-}GaCp^*)_2$ cluster (**2**) is evidently a result of the hemilabile vinyl function substitution for GaCp* followed by the rearrangement of the ligand sphere to give the face-bridging coordination of the GaCp* moiety (Figure 3). The substitution does not change the electron count for **2**, which is in agreement with the *closo* octahedral structure of the cluster framework. In contrast to **1** the phosphane ligand is only coordinated through the phosphorus atom, occupying a terminal position at the Rh(6) center. Possible coordination of the vinyl double bond to either Rh(4) or Rh(5) is obviously prevented by steric hindrance from the Ga(2)Cp* ligand. Local changes of the cluster geometry in **2** are in line with the regular effects of face-bridging GaCp*[13,14] and terminal phosphane ligands.[21] Metal–metal distances inside the rhodium triangles capped by GaCp* are significantly elongated (d^{av} = 2.824 Å) compared with the bond lengths of the rest of the octahedron (d^{av} = 2.783 Å). In the latter group the two bonds *cis* to the phosphane ligand are the longest (see Table 1), which is consistent with the general trend observed in the substituted $Rh_6(CO)_{16}$ derivatives.[21] The NMR spectroscopic data of **2** indicate that the structure found in the solid state remains unchanged in solution. The ^1H NMR spectrum of this cluster displays a broad multiplet of phenyl rings centered at 7.5 ppm, two singlets of slightly inequivalent Cp* methyl groups (2.17 and 2.19 ppm), and three resonances of the vinyl protons {δ =5.02 ppm [H(34)], 5.83 ppm [H(35b)], and 6.61 ppm [H(35a)]}, which are considerably low-field shifted compared with the spectrum of the coordinated vinyl fragment in **1** (see Experimental Section) and in $Rh_6(CO)_{14}(\mu,\kappa^3\text{-}Ph_2PCH{=}CH_2)$,[15] and demonstrate a very good agreement with the proton NMR spectrum of free diphenylvinylphosphane (see Figure S2). This observation clearly indicates that in solution the vinyl functionality remains uncoordinated as found in the solid state.

The ^{13}C NMR spectrum (see Experimental Section and Figure S3 in Supporting Information file) also fits well the structure found in the solid state. The spectrum displays resonances of two phenyl rings and the signals of inequivalent GaCp* ligands. The spectroscopic pattern observed in the carbonyl region of the spectrum displays three doublets and two dd resonances of terminal CO groups together with a quartet of the face bridging ligand that is in agreement with the presence of the symmetry plane through the Rh(1), Rh(6), C(33), and P(1) atoms. Additional phosphorus–car-

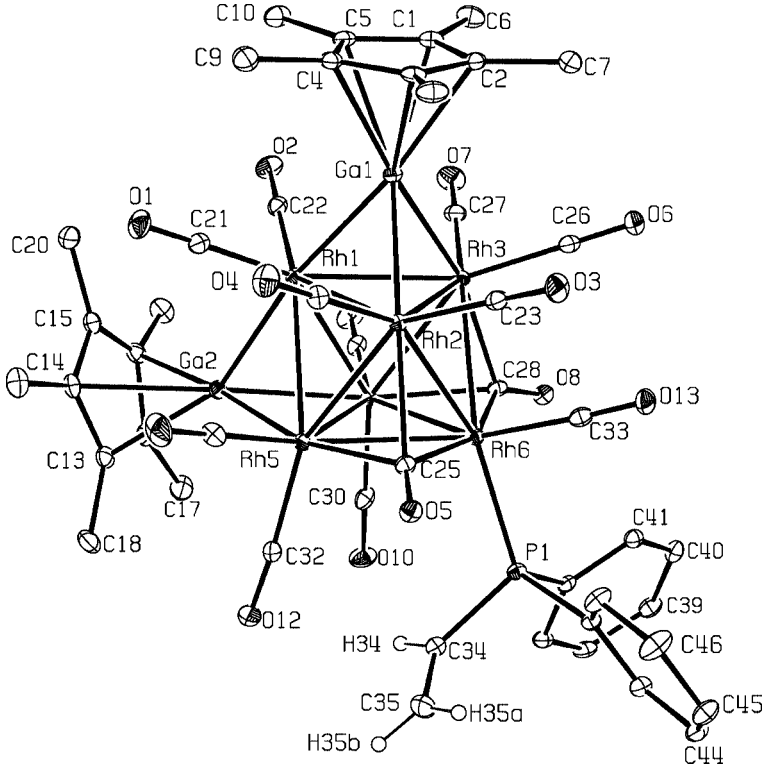

Figure 3. The ORTEP view of the $Rh_6(CO)_{13}(\mu,\kappa^1\text{-}Ph_2PC_2H_3)(\mu_3\text{-}GaCp^*)_2$ (**2**). Thermal ellipsoids are drawn at the 50% level.

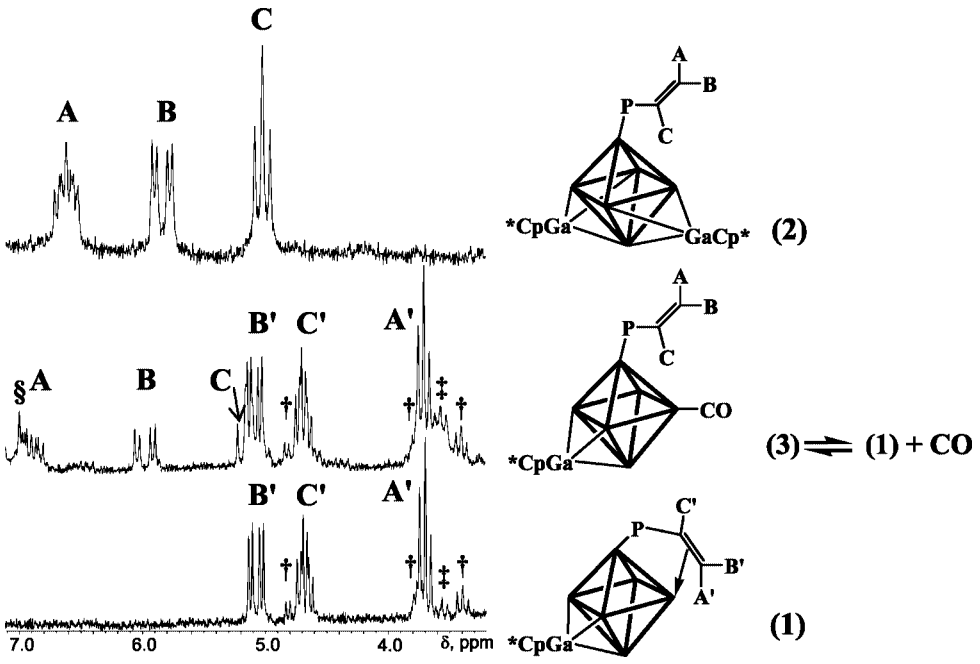

Figure 4. ^{1}H NMR spectra of **1**, **2**, and **3**; $CDCl_3$, 25 °C. The structures of the corresponding molecules are schematically shown on the right side of the figure. The admixture of the $Rh_6(CO)_{14}(\mu,\kappa^3\text{-}Ph_2PC_2H_3)$ starting cluster is marked by ‡. The signals of minor isomer **1** are marked by †. A signal of an unidentified impurity is marked by §.

bon couplings $^2J_{P–C(33)}$ and $^3J_{P–C(24,27)}$ are completely consistent with the stereochemistry of the intervening nuclei. It is interesting to note that this molecule is stereochemically rigid at room temperature in contrast with the $Rh_6(CO)_{15}PR_3$ derivatives that display low-temperature exchange between terminal and face-bridging CO groups bonded to the phosphane substituted rhodium atoms.[25] A similar C(33)O ↔ C(28)O, C(25)O exchange is still mechanistically possible in **2** but the electronic effect of the μ_3-GaCp* ligands in some way enlarges the barrier of these dynamics.

It has to be noted that the closest analogs of the starting cluster $[Rh_6(CO)_{14}(\mu\text{-dppm})]$ and $Rh_6(CO)_{14}(\mu,\kappa^2\text{-}Ph_2PPy)$, which contain non-hemilabile bridging phosphanes,[15,22] do not react with GaCp*, neither in the presence of Me_3NO nor under heating up to 50 °C. These observations stress a crucial role of the vinyl function hemilability in the chemistry under study. Initial coordination of the gallium ligand is at the terminal vacancy and this is followed by its migration into the thermodynamically stable face-bridging position. At the first stage this migration is accompanied by the recoordination of the vinyl function to keep it apart from the GaCp* moiety as shown in Figure 4. In the case of the cluster **2** the recoordination is sterically hindered because all available edge-bridging (with respect to phosphorus) positions are adjacent to μ_3-GaCp* ligands. This keeps the vinyl function in **2** uncoordinated.

Hemilabile behavior of the vinylphosphane in **1** was confirmed by the reaction of this cluster with gaseous CO. Saturation of the $CDCl_3$ solution of **1** with CO followed by the proton (Figure 4) and ^{31}P NMR (Figure S4) spectroscopic measurements showed that under these conditions **1** exists in equilibrium with the CO adduct **3**. Three multiplets of the vinyl protons in the adduct are very similar in location to those of cluster **2**, as are the spin-spin couplings (see Experimental Section), which clearly points to decoordination of the vinyl moiety. The ^{31}P NMR spectrum of the CO saturated solution of **1** is also very similar to that of $Rh_6(CO)_{14}(\mu,\kappa^3\text{-}Ph_2PCH{=}CH_2)$ under similar conditions (Figure S4). It was shown earlier[15] that the latter cluster easily substitutes the vinyl functionality with CO and similar spectroscopic characteristics of CO saturated solutions of these clusters implies a similarity in the chemistry that has occurred. A relative amount of the adduct **3** is ca 10–15% and purging of the reaction mixture with argon easily converts **3** into **1**.

In conclusion, this study has shown that hemilabile ligands in cluster complexes may provide easy access to various substituted products including those that contain such unusual substituents as GaCp* moieties. The presence of additional phosphane ligands in the coordination sphere of the starting cluster determines the stoichiometry of the products and their stereochemistry because of the mutual influence of the phosphane and incoming ligands.

Experimental Section

General Comments: All operations were carried out under an atmosphere of dry argon using standard Schlenk techniques. All solvents were distilled under an inert atmosphere over the appropriate drying agents prior to use. Commercial grade $Ph_2PC_2H_3$ (Aldrich) was used without additional purification. The starting $Rh_6(CO)_{14}(Ph_2PC_2H_3)$[15] cluster and the GaCp*[26] complex were synthesized according to literature procedures. Infrared spectra were recorded using a Specord M80 spectrometer. ^{1}H, ^{13}C{^{1}H}, and ^{31}P{^{1}H}

NMR spectra were recorded in C_6D_6 and $CDCl_3$ at room temperature using a Bruker DPX-300 instrument. The chemical shifts were referenced to residual solvent resonances for the ^1H and ^{13}C NMR spectra and external 85% H_3PO_4 for the ^{31}P NMR spectra. Microanalyses were carried out in the Microanalytical Laboratory of St. Petersburg State University. FAB mass spectra were obtained with a VG Autospec instrument (Institute of Organic Chemistry, University of Heidelberg). The observed isotopic distribution patterns completely fit the calculated ones. The products were purified by column chromatography on silica, 5–40 mesh, Merck Kieselgel 60.

Synthesis of 1 and 2: $Rh_6(CO)_{14}(Ph_2PC_2H_3)$ (50 mg, 0.041 mmol) was dissolved in THF (20 mL) and frozen in a Schlenk vessel by liquid nitrogen. A glass capillary tube with GaCp* (20 mg, 0.097 mmol) was placed into the vessel. The reaction mixture was warmed to room temperature under vigorous stirring, which broke the capillary tube immediately. After an hour all volatile components of the reaction mixture were removed in vacuo to leave a brown-greenish precipitate, which was washed with *n*-hexane (10 mL) and dried once more in vacuo. The residue was redissolved in CH_2Cl_2 (10 mL) and diluted with *n*-hexane (30 mL). The solution was transferred onto a chromatographic column (3 × 10 cm). Elution with *n*-hexane/CH_2Cl_2 (3:1 v/v) gave the following bands in the order of elution: $Rh_6(CO)_{12}(GaCp^*)_4$, $Rh_6(CO)_{13}(GaCp^*)_3$, $Rh_6(CO)_{13}(Ph_2PC_2H_3)(GaCp^*)_2$ (**2**, 23 mg), $Rh_6(CO)_{15}(GaCp^*)$, and $Rh_6(CO)_{13}(Ph_2PC_2H_3)(GaCp^*)$ (**1**, 14 mg). Removal of the solvents from the third and fifth bands gave brown and green-brown crystalline materials, respectively. The other components of the reaction mixture were identified by comparison of their IR spectroscopic characteristics with the literature data.[13]

1: IR (CH_2Cl_2): $\tilde{\nu}_{max}$(CO) = 2076 (w), 2052 (s), 2040 (s), 2016 (m), 1780 (m br), 1768 (m br) cm^{-1}. ^1H NMR (300 MHz, $CDCl_3$): **Major isomer:** δ = 2.24 (s, 15 H, C_5Me_5), 3.67 [ddd, $^2J_{H(24a)-H(25a)}$ = 2.0, $^3J_{H(24a)-H(26a)}$ = 14.0, $^3J_{H(24a)-P(1a)}$ = 14.0, 1 H, *H*(24a)], 4.68 [ddd, $^3J_{H(26a)-H(24a)}$ = 14.0, $^2J_{H(26a)-P(1a)}$= 14.0, $^3J_{H(26a)-H(25a)}$ = 10.0, 1 H, *H*(26a)], 5.07 [ddd, $^3J_{H(26a)-H(25a)}$ = 10.0, $^2J_{H(25a)-H(24a)}$ = 2.0, $^3J_{H(25a)-P(1a)}$ = 26.0, 1 H, *H*(25a)], 7.36–8.14 (m, 10 H, *phenyl rings*) ppm. **Minor isomer:** δ = 2.25 (s, 15 H, C_5Me_5), 3.40 [dd, $^3J_{H(24b)-H(26b)}$ = 14.0, $^3J_{H(24b)-P(1b)}$ = 14.0, 1 H, *H*(24b)], 3.74 [ddd, $^3J_{H(26b)-H(25b)}$ = 10.0, $^2J_{H(26b)-P(1b)}$ = 14.0, $^3J_{H(26b)-H(24b)}$ = 10.0, 1 H, *H*(26b)], 4.77 [dd, $^3J_{H(25b)-H(26b)}$ = 10.0, $^3J_{H(25b)-P(1b)}$ = 26.0, 1 H, *H*(25b)], 7.36–8.14 (m, 10 H, *phenyl rings*) ppm. $^{31}P\{^1H\}$ NMR (121 MHz, $CDCl_3$) **Major isomer:** δ = 17.0 [dd, $^1J_{Rh(5)-P(1a)}$ = 130, $^2J_{Rh(2)-P(1a)}$ = 7, 1 P, *P*(1a)] ppm. **Minor isomer:** δ = 27.0 [d, $^1J_{Rh(5)-P(1b)}$ = 122, 1 P, *P*(1b)] ppm. $C_{37}H_{28}GaO_{13}PRh_6$: calcd. C 31.77, H 2.02; found C 31.98, H 2.47. MS FAB$^+$: 1397 (M^+), 1369 (M^+ – 1 CO), 1285 (M^+ – 4 CO), 1257 (M^+ – 5 CO), 1229 (M^+ – 6 CO), 1201 (M^+ – 7 CO), 1173 (M^+ – 8 CO). Single crystals of **1** suitable for X-ray studies were obtained by gas-phase diffusion of *n*-hexane into CH_2Cl_2 solution under a nitrogen atmosphere.

2: IR (CH_2Cl_2): $\tilde{\nu}_{max}$(CO) = 2040 (vs), 2024 (s), 2000 (m), 1772 (m br), 1756 (m br) cm^{-1}. ^1H NMR (300 MHz, $CDCl_3$): δ = 2.17 (s, 15 H, C_5Me_5), 2.19 (s, 15 H, C_5Me_5), 5.02 [dd, $^3J_{H(34)-H(35a)}$ = 17.0, $^2J_{H(34)-P}$ = 20.0, 1 H, *H*(34)], 5.83 [dd, $^3J_{H(35b)-P}$ = 36.0, $^2J_{H(35b)-H(35a)}$ = 12.0, 1 H, *H*(35b)], 6.61 [ddd, $^3J_{H(34)-H(35a)}$ = 17.0, $^2J_{H(35b)-H(35a)}$ = 12.0, $^2J_{H(35a)-P}$ = 28.0, 1 H, *H*(35a)], 7.38–7.68 (m, 10 H, *phenyl rings*) ppm. $^{31}C\{^1H\}$ NMR (125 MHz, $CDCl_3$, ambient temperature): δ = 11.03 (s, C_5Me_5), 11.15 (s, C_5Me_5), 119.19 (s, C_5Me_5), 119.38 (s, C_5Me_5), 128.80 (d, $^1J_{C-P}$ = 10, 4 C, $C_{ortho/meta}$), 131.15 (s, 2 C, C_{para}), 134.14 (d, $^1J_{C-P}$ = 10, 4 C, $C_{meta/ortho}$), 184.27 (d, $^1J_{C-Rh}$ = 64, 2 CO, *t*-*CO*), 184.73 (d, $^1J_{C-Rh}$ = 64, 2 CO, *t*-*CO*), 185.84 (dd, $^1J_{C-Rh}$ = 70, $^2J_{C-P}$ = 13, 1CO, *t*-*C*(33)*O*), 186.53 [dd, $^1J_{C-Rh}$ = 68, $^3J_{C-P}$ = 19, 2 CO, *t*-*C*(24)*O* and *t*-*C*(27)*O*], 187.23 (d, $^1J_{C-Rh}$ = 62, 2 CO, *t*-*CO*), 188.08 (d, $^1J_{C-Rh}$ = 65, 2 CO, *t*-*CO*), 253.93 (ddd, $^1J_{C-Rh}$ = 21, $^1J_{C-Rh}$ = 28, $^1J_{C-Rh}$ = 32, 2 CO, μ_3-*CO*) ppm. $^{31}P\{^1H\}$ NMR (121 MHz, $CDCl_3$, ambient temperature): δ = 21.0 [d, $^1J_{Rh-P}$ = 131, *P*(1)] ppm. $C_{47}H_{43}Ga_2O_{13}PRh_6$ + C_6H_{14}: calcd. C 37.67, H 3.40; found C 36.99, H 3.77. MS FAB$^+$: 1604 (M^+), 1549 (M^+ – 2 CO), 1436 (M^+ – 6 CO), 1408 (M^+ – 7 CO), 1380 (M^+ – 8 CO), 1352 (M^+ – 9 CO), 1324 (M^+ – 10 CO). Single crystals of **2** suitable for X-ray studies were obtained by gas-phase diffusion of *n*-hexane into CH_2Cl_2 solution under a nitrogen atmosphere.

Reaction of 1 with Gaseous CO: A solution of the $Rh_6(CO)_{13}(Ph_2PC_2H_3)(GaCp^*)$ in $CDCl_3$ (0.5 cm^3) in a standard NMR tube (5 mm) was saturated with gaseous CO at room temperature. ^1H and ^{31}P NMR spectra showed the formation of a new $Rh_6(CO)_{14}(\kappa^1\text{-}Ph_2PC_2H_3)(GaCp^*)$ (**3**) complex, which was characterized by ^1H and $^{31}P\{^1H\}$ NMR spectroscopy. Under these conditions the

Table 2. Crystallographic data for **1** and **2**.

Empirical formula	$C_{37}H_{28}Ga_1O_{13}PRh_6$ (**1**)	$C_{47}H_{43}Ga_2O_{13}PRh_6 \cdot CH_2Cl_2$ (**2**)
Formula mass [g mol^{-1}]	1398.74	1688.61
Temperature [K]	100(2)	100
Wavelength [Å]	0.71073	0.71073
Space group	$P2_1/c$	$P2_1/c$
a [Å]	20.4099(16)	20.0500(2)
b [Å]	10.8774(9)	14.85500(10)
c [Å]	21.9594(14)	18.6900(2)
β [°]	122.238(5)	102.6100(5)
V [Å^3]	4123.6(5)	5432.40(9)
Z	4	4
Calculated density [g cm^{-3}]	2.253	2.065
F(000)	2680	3272
Crystal size [mm]	0.15 × 0.15 × 0.10	0.30 × 0.30 × 0.05
θ range for data collection [°]	1.85 to 32.02	2.9 to 27.5
Index ranges	$-30 \le h \le 27$, $-16 \le k \le 0$, $-32 \le l \le 26$	$-26 \le h \le 25$, $-19 \le k \le 19$, $-24 \le l \le 24$
Reflections collected/unique	73119/14142 [*R*(int) = 0.0440]	130198/12404 [*R*(int) = 0.050]
Completeness to:	θ = 32.02° 98.5%	θ = 27.5° 99.7%
Data/restraints/parameters	14142/0/574	12404/0/659
Goodness-of-fit on F^2	1.076	1.062
Final *R* indices [$I > 2(I)$]	R_1 = 0.0303, wR_2 = 0.0656	R_1 = 0.0262, wR_2 = 0.0595
R indices (all data)	R_1 = 0.0445, wR_2 = 0.0703	R_1 = 0.0339, wR_2 = 0.0620
Largest diff. peak [e Å^{-3}]	0.151, 1.111	1.119

ratio **1/3** equals 7:1. The cluster **3** is unstable and readily converts back to **1** after purging the CO saturated solution with argon.

3: ^{1}H NMR (300 MHz, $CDCl_3$, ambient temperature): δ = 2.21 (s, 15 H, C_5Me_5), 5.15 {dd, $^3J_{H(26)-H(24)}$ 18.5, $^2J_{H(26)-P(1)}$ 20.0, 1 H, *H*(26)], 5.97 [dd, $^3J_{H(25)-P(1)}$ 37.2, $^2J_{H(25)-H(24)}$ 12.2, 1 H, *H*(25)], 6.89 [ddd, $^3J_{H(26)-H(24)}$ 18.5, $^2J_{H(25)-H(24)}$ 12.2, $^2J_{H(24)-P(1)}$ 29.0, 1 H, *H*(24)], 7.36–8.14 (m, 10 H, *phenyl rings*) ppm. $^{31}P\{^1H\}$ NMR (121 MHz, $CDCl_3$, ambient temperature): δ = 20.0 [d, $^1J_{Rh(5)-P}$ = 131, *P*(1)] ppm. A resolution enhancement procedure was used to obtain spin-spin coupling constants in the ^{1}H spectrum of **3**.

X-ray Crystal Structure Determinations

Complex 1: Intensity data were collected at low temperature with a Bruker AXS Smart1000 CCD diffractometer, and corrected for absorption and other effects.[27] The structure was solved by the Patterson method and refined by full-matrix least-squares based on F^2. All non-hydrogen atoms were given anisotropic displacement parameters. Hydrogen atoms were inserted in calculated positions. The calculations were performed using the programs DIRDIF[27] and SHELXL.[28]

Complex 2: Single crystals of **2** (dimensions $0.30 \times 0.30 \times 0.05$ mm) were used for data collection at 100 K with a Bruker-Nonius KappaCCD diffractometer with graphite-monochromated Mo-K_α radiation (λ = 0.71073 Å). The structure was solved by direct methods. The program package used was SHELXL 97.[28] Full-matrix least-squares refinement on F^2 was carried out anisotropically for the non-hydrogen atoms. Hydrogen atoms were included at calculated positions using a riding model.

The crystallographic data are summarized in Table 2. Selected bond lengths and angles for **1** and **2** are shown in Table 1.

Supporting Information (see also the footnote on the first page of this article): VT ^{1}H NMR spectra of **1**, ^{1}H NMR spectrum of free diphenylvinylphosphane, ^{13}C NMR spectrum of **2**, ^{31}P NMR spectra of **1**, **2** and **3**.

Acknowledgments

Financial support from the Alexander von Humboldt Foundation (for E. V. G.) and RFBR (Grant 05-03-33266) is gratefully acknowledged.

[1] C. Gemel, T. Steinke, M. Cokoja, A. Kempter, R. A. Fischer, *Eur. J. Inorg. Chem.* **2004**, 4161–4176.
[2] G. Linti, H. Schnöckel, *Coord. Chem. Rev.* **2000**, *206–207*, 285–319.
[3] G. Linti, W. Kostler, *Chem. Eur. J.* **1998**, *4*, 942–949.
[4] P. Jutzi, B. Neumann, G. Reumann, H.-G. Stammler, *Organometallics* **1998**, *17*, 1305–1314.
[5] P. Jutzi, B. Neumann, L. O. Schebaum, A. Stammler, H.-G. Stammler, *Organometallics* **2000**, *19*, 1445–1447.
[6] P. Jutzi, B. Neumann, L. O. Schebaum, A. Stammler, H.-G. Stammler, *Organometallics* **1999**, *18*, 4462–4464.
[7] D. Weiss, T. Steinke, M. Winter, R. A. Fischer, N. Frohlich, J. Uddin, G. Frenking, *Organometallics* **2000**, *19*, 4583–4588.
[8] H. Folsing, O. Segnitz, U. Bossek, K. Merz, M. Winter, R. A. Fischer, *J. Organomet. Chem.* **2000**, *606*, 132–140.
[9] P. Jutzi, N. Lenze, B. Neumann, H.-G. Stammler, *Angew. Chem. Int. Ed.* **2001**, *40*, 1424–1427.
[10] D. Weiss, M. Winter, R. A. Fischer, C. Yu, K. Wichmann, G. Frenking, *Chem. Commun.* **2000**, 2495–2496.
[11] M. Cokoja, T. Steinke, C. Gemel, T. Welzel, M. Winter, K. Merz, R. A. Fischer, *J. Organomet. Chem.* **2003**, *684*, 277–286.
[12] C. Gemel, T. Steinke, D. Weiss, M. Cokoja, M. Winter, R. A. Fischer, *Organometallics* **2003**, *22*, 2705–2710.
[13] E. V. Grachova, P. Jutzi, B. Neumann, L. O. Schebaum, H.-G. Stammler, S. P. Tunik, *J. Chem. Soc., Dalton Trans.* **2002**, 302–304.
[14] E. V. Grachova, P. Jutzi, B. Neumann, H.-G. Stammler, *Dalton Trans.* **2005**, 3614–3616.
[15] E. V. Grachova, M. Haukka, B. T. Heaton, E. Nordlander, T. A. Pakkanen, I. S. Podkorytov, S. P. Tunik, *Dalton Trans.* **2003**, 2468–2473.
[16] N. Lugan, F. Laurent, G. Lavigne, T. P. Newcomb, E. W. Liimatta, J. J. Bonnet, *Organometallics* **1992**, *11*, 1351–1363.
[17] E. Rosenberg, L. Milone, R. Gobetto, D. Osella, K. Hardcastle, S. Hajela, K. Moizeau, M. Day, E. Wolf, D. Espitia, *Organometallics* **1997**, *16*, 2665–2673.
[18] J. A. Cabeza, *Eur. J. Inorg. Chem.* **2002**, 1559–1570.
[19] M. McPartlin, D. M. P. Mingos, *Polyhedron* **1984**, *3*, 1321–1328.
[20] M. S. Owen, *Polyhedron* **1988**, *7*, 253.
[21] D. H. Farrar, E. V. Grachova, A. Lough, C. Patirana, A. J. Poe, S. P. Tunik, *J. Chem. Soc., Dalton Trans.* **2001**, 2015–2019.
[22] D. H. Farrar, E. V. Grachova, M. Haukka, B. T. Heaton, J. A. Iggo, T. A. Pakkanen, I. S. Podkorytov, S. P. Tunik, *Inorg. Chim. Acta* **2003**, *354*, 11–20.
[23] S. P. Tunik, I. O. Koshevoy, A. J. Poe, D. H. Farrar, E. Nordlander, M. Haukka, T. A. Pakkanen, *Dalton Trans.* **2003**, 2457–2467.
[24] D. V. Krupenya, S. I. Selivanov, S. P. Tunik, M. Haukka, T. A. Pakkanen, *Dalton Trans.* **2004**, 2541–2549.
[25] E. V. Grachova, B. T. Heaton, J. A. Iggo, I. S. Podkorytov, D. J. Smawfield, S. P. Tunik, R. Whyman, *J. Chem. Soc., Dalton Trans.* **2001**, 3303–3311.
[26] P. Jutzi, L. O. Schebaum, *J. Organomet. Chem.* **2002**, *654*, 176–179.
[27] P. T. Beurskens, G. Beurskens, R. de Gelder, S. Garcia-Granda, R. O. Gould, R. Israel, J. M. M. Smits, in: *The DIRDIF-99 program system*, The Netherlands, **1999**.
[28] G. M. Sheldrick, in: *SHELXL97, Program for Crystal Structure Refinement*, **1997**.

Received: July 28, 2006
Published Online: November 9, 2006

